GIDA
THE JOURNAL OF FOOD
E-ISSN 1309-6273, ISSN 1300-3070

Research / Araştırma
GIDA (2020) 45(3) 600-611
doi: 10.15237/gida.GD20057

IN VITRO CYTOTOXICITY ANALYSIS AND SYNTHESIS OF BIOCIDAL ALLICIN/MT/MMA/PEG/POSS NANOCOMPOSITES FOR THE FOOD PACKAGING

Gülay Baysal*
Istanbul Aydin University, Faculty of Engineering, Department of Food Engineering, Istanbul, Turkey

Received /Geliş: 28.04.2020; *Accepted* / Kabul: 10.06.2020; *Published online* / Online baskı: 16.06.2020

Baysal, G. (2020). In vitro cytotoxicity analysis and synthesis of biocidal Allicin/MT/MMA/PEG/POSS nanocomposites for the food packaging. GIDA (2020) 45(3) 600-611 doi: 10.15237/gida.GD20057

Baysal, G. (2020). In vitro cytotoxicity analysis and synthesis of biocidal Allicin/MT/MMA/PEG/POSS nanocomposites for the food packaging. GIDA (2020) 45(3) 600-611 doi: 10.15237/gida.GD20057

ABSTRACT
In this study, the new nanocomposites were synthesized using antibacterial and antioxidant curcumin (Cr) and allicin (Ac), the high mechanical strength montmorillonite clay (Mt) and biocompatible methylmethacrylate (MMA), polyethylene glycol (PEG) and polyocta-hedral oligomeric silsesquioxanes (POSS) polymers. Firstly, monomer 1 was synthesized by using Ag^+-montmorillonite, the curcumin extract and POSS, then the synthesized monomer 1 was interacted with MMA and PEG polymers, and nanocomposites were synthesized. The synthesized nanocomposites were analyzed by using the methods of Fourier Transform Infrared Spectroscopy (FTIR), X-ray diffraction (XRD) and scanning electron microscopy (SEM). After this, the inhibition zones and the surface activity resistances of the nanocomposites were analyzed against the bacteria *Escherichia coli (E. coli)*, *Listeria monocytogenes (L. monocytogenes)*, *Salmonella* and *Staphylococcus aureus (S.aureus)* and carried out biocompatibility analysis. According to the analysis results, the nanocomposites have been found to have the strong antibacterial resistance and biocompatibility.
Keywords: Surface activity, biocompatibility, the curcumin, biopolimers, the allicin.

GIDA AMBALAJI İÇİN BİYOSİDAL ALLİSİN / MT / MMA / PEG / POSS NANOKOMOZİTLERİNİN SENTEZİ VE İN VİTRO SİTOTOKSİSİTE ANALİZİ

ÖZ
Bu çalışmada, antibakteriyel ve antioksidan kurkumin (Cr) ve allisin (Ac), yüksek mekanik mukavemetli montmorillonit kili (Mt) ve biyouyumlu polimetilmetakrilat (PMMA), polietilen glikol (PEG) ve polioktahedral oligomerik silseskioksan (POSS) polimerleri kullanılarak yeni nanokompozitler sentezlenmiştir. Öncelikle, Ag^+-montmorillonit, kurkumin ekstraktı ve POSS kullanılarak monomer 1 sentezlendi, daha sonra sentezlenen monomer 1, MMA ve PEG polimerleri ile etkileştirilmiş, ve nanokompozitler sentezlenmiştir. Sentezlenen yüzey nanokompozitler, Fourier Transform Kızılötesi Spektroskopisi (FTIR), X-ışını kırınımı (XRD) ve taramalı elektron mikroskopisi (SEM) yöntemleri kullanılarak analiz edilmiştir. Daha sonra, nanokompozitlerin inhibisyon bölgesi alanları ve yüzey aktivite dirençleri, *Escherichia coli (E.coli), Listeria monocytogenes (L. monocytogenes), Salmonella ve Staphylococcus aureus (S.aureus)* bakterilerine karşı analiz edilmiş ve biyouyumluluk testleri yapılmıştır. Analiz sonuçlarına göre, nanokompozitlerin güçlü antibakteriyel dirence ve biyouyumluluğa sahip olduğu bulunmuştur.
Anahtar Kelimeler: Yüzey aktivitesi, biyouyumluluk, kurkumin, biyopolimerler, allisin.

* *Corresponding author* / Yazışmalardan sorumlu yazar
✉ gulaybaysal@aydin.edu.tr, ✆ (+90) 444 14 28-22409 🖷 (+90) 212 425 5759
Gülay Baysal; ORCID no: 0000-0001-7081-1472

INTRODUCTION

Biopolymers have been the focus of interest in the industrial and health sectors due to the rapidly decreasing oil resources in the world and the toxic and carcinogenic effects of synthetic petroleum-derived polymers (Söğüt et al., 2017). In the structure of biopolymer-based nanocomposites, biopolymers are used as matrix and nanoparticles, nanofiller materials, nanotubes and nanoclays are used as filling materials. Thus, it is possible to synthesize nanocomposites of different structures and properties. The silver-based multilayer biocompatible nanocomposites are widely used in a wide range of applications. Nanomaterials are used in many fields such as; the biosensors, bone cements, anticarcinogenic materials, (Dag et al., 2019) antibacterial products in biomedical applications (Söğüt et al., 2017), controlled release systems in pharmaceutical industry, optical applications, dielectric material in electrical applications, (Rostami et al., 2019) antimicrobial (Baysal and Çelik, 2018) and antioxidant (Rostami et al., 2019) materials in packaging systems in the food industry. The turmeric plant extract curcumin is a phenolic compound and has a strong antimicrobial effect (Dhivya et al., 2017). The allium sativum is among the most important chemical compounds found in garlic. According to the literature, Garlic plant has anti-bacterial, anti-fungal (Özçelik et al., 2007), anti-parasitic and anticarcinogenic properties that have been proven (Cheng and Huang, 2018). PMMA, POSS and PEG used in this study are biocompatible polymers that are miscible with each other. The C=O group of PMMA essentially interacts with the terminal -OH group of PEG to develop C=O ···H-O species (Shinzawa and Mizukada, 2018).

Although PLA blends with PC and PMMA are not biodegradable, they can be preferred for making durable goods with increased bio-based content for food packaging. According to the researches, it is seen that the modified PMMA composites can be a promising candidate for active food packaging. In particular, mechanical stability, gas barrier properties and antibacterial properties support studies in this area (Abdel Rehim et al., 2020; Deng et al., 2017). PMMA is particularly important for mixing with PHA and PHB since it is a biocompatible polymer that allows the polyester tobe used in the food packaging. Besides, PMMA is one of the important materials used in a variety ofoptical devices such as polymer optical fibers, optical films forliquid-crystal displays, optical disks, lenses, etc. because of itsexceptional clarity in the visible range (Yalcın et al. 2006; Abdel Rehim et al., 2020).

In this study, silver, turmeric extract curcumin and garlic extract allicin, montmorillonite clay, POSS, MMA and polyethylene glycol as biomaterials were interacted by chemical synthesis and developed a multifunctional material in the areas of surface-active, biocompatible and mechanical strength. The surface activity and antibacterial properties of synthesized nanocomposites against *S. aureus, L. monocytogenes, Salmonella* and *E. coli* bacteria were analyzed and examined biocompatibility tests. Figure 1 shows the molecular structure of curcumin (a) and allicin (b).

MATERIALS AND METHODS

Materials

Curcuma longa (turmeric, molecular weight: 368.38 g/mol, curcuminoid content ≥ 94%), garlic extract (Cas number: 8000-78-0, the allium sativum < =100%), methyl methacrylate, dimethylformamide, diethyl ether, polyethylene glycol monoacrylate octaphenyl-polyhedral oligomeric silsesquioxane (POSS, Molecular weight: 1033.51 g/mol), silver nitrate ($AgNO_3$) were purchased from Sigma-Aldrich (Germany). Na^+-Montmorillonite was provided by Southern Clay Products Inc. (U.S.A.). The physical and chemical properties of Mt are shown in Table 1.

Nanocomposites synthesis

Modification of Ag^+-Montmorillonite (Mt)

The silver nitrate solution (0.05 M, 50 mL) was added to the sodium montmorillonite (1.0 g) and mixed for 3 h at 25 °C in a dark room. The mixture was then centrifuged at 3000 rpm for 20 min. The liquid phase from the obtained product was decanted and then washed with distilled water for 4-5 times to remove the nitrate ions from the precipitate. The final product was waited to dry in a dark environment under room conditions (Sohrabnezhad et al., 2016).

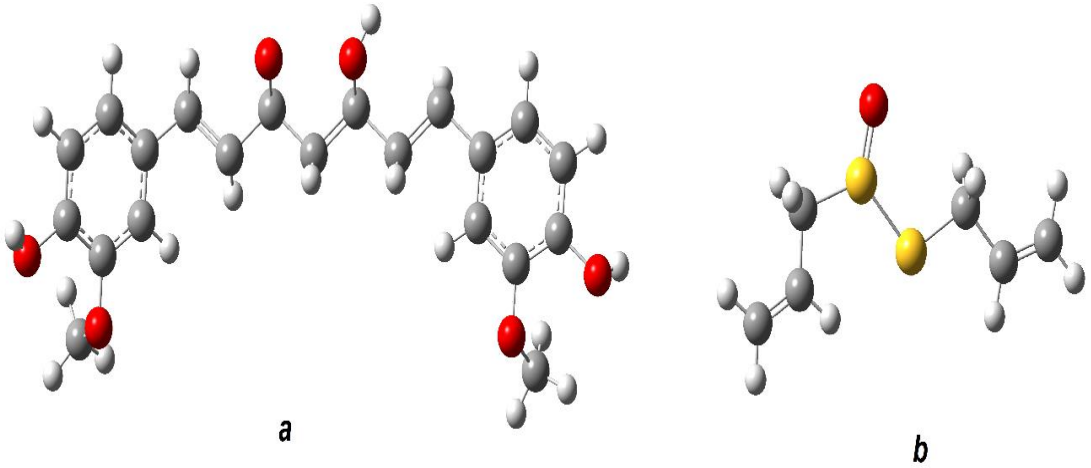

Figure 1. The molecular structure of curcumin (a) and allicin (b)

Table 1. The physical and chemical properties of Na^+- Mt.

Molecule formula	$(Na, Ca)_{0.33}(Al, Mg)_2 Si_4O_{10}(OH)_26H_2O$
The density (g. cm^{-3})	2.86
pH (%3 solution)	8
The specific surface area ($m^2.g^{-1}$)	750
CEC (meg.100 g^{-1})	92
The percent of composition (%)	1.40 Na, 2.44 Ca, 9.99 Al, 8.88 Mg, 20.7 Si, 35.53 O, 0.37 H

Organoclay Synthesis

Ag^+-Mt (2. 0 g) was added to a mixture of deionized water-ethanol (v: v (1: 1) 100 mL) and stirred for 1 h at room temperature. In a separate apparatus, curcumin (2. 0 g) were mixed with a water-ethanol mixture prepared in a ratio of 1: 1 and stirred at room temperature for 1 h. The two different solutions prepared were mixed with each other and stirring continued for 24 h. After 24 h, the solution mixture was passed through filter paper and precipitate was washed with water/ethanol mixture 3-4 times on average. The resulting filtrate was dried in an oven at 70 °C for 24 h. The same operations were performed in allicin. The synthesized product was named Ag^+-Mt-Cr and Ag^+-Mt-Ac (Baysal and Çelik, 2018).

Preparation of the Ag^+-Montmorillonite-Curcumin extract-POSS (Monomer1)

Ag^+-Mt (3.0 g) was mixed into 250 mL of distilled water for 2 h under room conditions. POSS and curcumin (3.0 g) were then added to 10 mL of ethanol that did not contain any water and mixed for 5 min, followed by adding 2 mL of acetic acid and mixing for 24 h at 70 °C. The final product was centrifuged at 3500 rpm for 15 min and the supernatant was decanted. The precipitate that was obtained was washed 3 times with a mixture of deionized water-ethanol (v: v (1:1)), filtered and left to dry under room conditions (Zhao et al., 2009).

Synthesis of nanocomposites 1, 2 and 3

Monomer 1 (1. 5 g), methylmethacrylate (6. 0 g), polyethylene glycol (0. 3 g) were added to 8 mL of dimethylformamide solvent. The solution was stirred at 60 °C for 5 h. After 5 h, the mixture was cooled, and 60 mL of diethyl ether were added to precipitate. The liquid phase was separated from the precipitate and the precipitate was dried with nitrogen and stored as a final product in the dark in a refrigerator and under nitrogen at +4 °C. Similarly, the three different nanocomposites were synthesized by changing chemical ratios and contents. Table 2 shows the chemical ratio of nanocomposites.

Table 2. The chemical ratio of nanocomposites (g)

	Ag^{+}-Mt-Ac	*Monomer1*	*MMA*	*PEG*
Composite 1		1,5	6	0,3
Composite 2		1,5	6	0,6
Composite 3	0,5	-	3	-

Characterization

The synthesized nanocomposites were observed and examined by using a JOEL JSM 5600 LV scanning electron microscope (SEM) with an accelerating beam at a voltage of 40 kV. FTIR spectra (Mattson 1000 infrared spectrophotometer) were measured in the wavenumber range of 4000–400 cm^{-1} at a resolution of 4 cm^{-1}. The crystallinity of the nanocomposites was examined by X-ray diffraction measurements (XRD). The Bragg's Law was used to calculate the distances between clay layers.

Biocidal Activity

The Surface Activity Analysis

The bacteria *E. coli, Salmonella, S. aureus*, and *L. monocytogenes* were inoculated onto Nutrient agar and incubated for 24 h at 37 °C in an aerobic setting. The cells were also spread in the same medium, and after 24 h, significant reductions in numbers of bacteria were observed around the disk the nanocomposite specimen was applied at inhibition concentrations. The surface activity performances of nanocomposites against bacteria were examined by using Zeiss Microscope at magnification scale of X40.

Antibacterial Analysis

The bacteria *E. coli, Salmonella, L. monocytogenes*, and *S. aureus* were inoculated onto Nutrient agar and incubated at 37 °C for 24 h in an aerobic setting by using the well diffusion method. The cells were also spread in the same medium, and after 24 h, the compounds created inhibition zones around the disk it was applied at inhibition concentrations was checked. The radii of the inhibition zones were measured in units of mm (Baysal and Çelik, 2018).

Biocompatibility Analysis

Samples were prepared by dissolving in water-based (Dulbecco's Modified Eagle's Medium) DMEM medium. Photometric reading was performed at 570 nm. In 96-well plates, the cell seeding was performed so that the L929 fibroblast cell line was 105 cells / mL and allowed to adhere to cells in a 37 °C CO_2 incubator for 24 h. After 24 h, the cell culture MTT (3- [4,5-Dimethylthiazole-2-yl] -2,5-diphenyltetrazolium bromide) viability test was performed. The results were calculated assuming that the negative control was 100% viable.

Statistical Analysis

In this research, Minitab 16 software was used for statistical analysis. Results are presented as the mean value ± standard deviation (SD). Statistical analysis is made using analysis of variance (one-way ANOVA with t test). and Tukey's test at a confidence level of 95% were used.

RESULTS AND DISCUSSION

FTIR Analysis

In FTIR spectra, polymethylmethacrylate (PMMA) exhibits C-H tensile bands around 2996, 2993, 2951, 2930, 2933, 2926 cm^{-1}. The wide band peaks seen at 3622-3473-3469 cm^{-1} are due to the axial stretching of the O-H groups forming the H bonds with the polymeric material. The characteristic peaks of PMMA represent the C = O carbonyl group around 1725, 1724 and 1672 cm^{-1}, the C-O vibration stresses around 1000-1119 cm^{-1}, the off-axis and in-axial C-O-C bending peaks of about 800-700 cm^{-1}. In the spectrum of composite 1 and composite 2, the peaks at 3069 and 3073 cm^{-1} are shown as C-H stresses of aromatic groups in the structure of curcumin. The peaks at 1437, 1433, 1432, 1386 and 1388 cm^{-1} represent the C-H and C-O tensile bands found in the structure of curcumin and allicin (Silva et al., 2019). Si-O-Si bonds in the clay structure are represented by the peaks seen in the 1000-1100 cm^{-1} range. Figure 2 shows FTIR spectra of nanocomposites 1, 2 and 3.

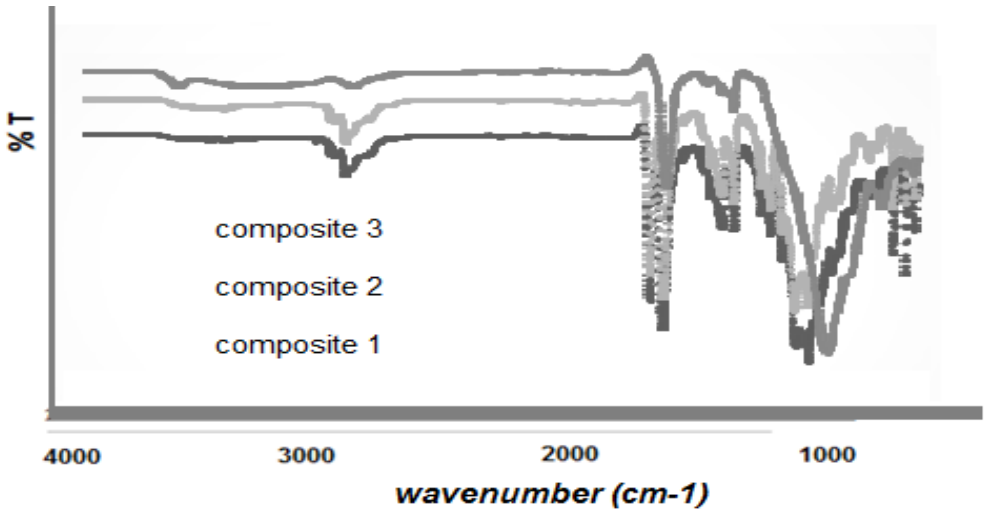

Figure 2. FTIR spectra of nanocomposites 1, 2 and 3.

XRD Analysis

Figure 3 shows the XRD spectra of composite 1, 2 and 3 samples. The d 001 spacing was calculated and listed in Table 3 from peak positions using Bragg's law equation $2d \sin\theta = n\lambda$. It is seen that the d-spacing for Mt (9.7A°) increased to 10.50°A. Because the clay was first modified with curcumin and allicin and then added to the synthesis step. Table 3 shows peak values of composite 1, 2 and 3 according to Baragg's law.

Table 3. Peak values of composite 1, 2 and 3 according to Baragg's law

	Pos. [°2Th.]	*Height [cts]*	*FWHM [°2Th.]*	*d-spacing [Å]*	*Rel. Int. [%]*
Composite 1	8.5009	59.28	0.2362	10.40173	11.35
Composite 2	8.3787	56.72	0.3542	10.55320	54.88
Composite 3	8.9161	47.80	0.2362	9.91823	37.63

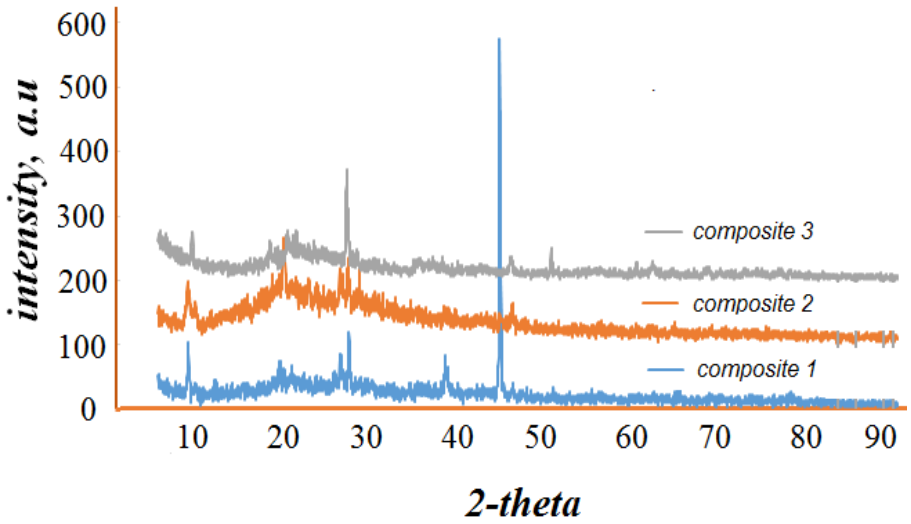

Figure 3. XRD spectra of nanocomposite 1, 2 and 3.

When XRD spectra are examined, Figure 3 shows the samples of the spectrum of exfoliated and intercalated composite structures. The composite 2 and 3 spectra show completely exfoliated structures, while composite 3 exfoliated and intercalated. The amorphous structure of PMMA in the synthesized composition appears to be supported by the compounds (Silva et al., 2019; Philip et al., 2019). In the case of composite 1, the organoclay did not completely lose its crystal structure when interacting with the polymer, but when the amount of PEG was increased, the structure showed a completely exfoliated character. This result can be interpreted as supporting the effect of PEG on an amorphous structure in PMMA and organoclay interaction.

SEM Analysis

Figure 4 shows SEM images of the surface morphology of pure PMMA and composite 3 samples at magnification scales of 10 to 200 μm, respectively.

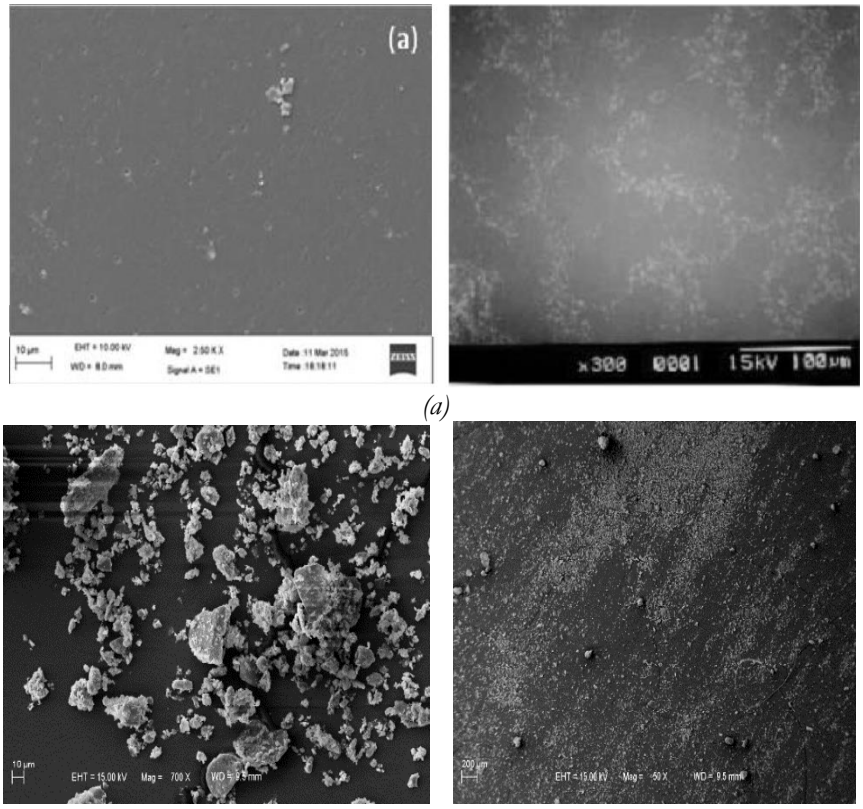

(a)

(b)

Figure 4. SEM images of pure PMMA (a) (Ravindar Reddy et al., 2019; Kim et al., 2004) and nanocomposite 3 (b)

In Figure 4 (a), the SEM image of PMMA (Ravindar Reddy et al., 2019; Kim et al., 2004) shows that the surface is homogeneous and smooth. In Figure 4 (b), the surface morphological image of the nanocomposite 3 sample shows that the surface is transformed into a rough and porous structure (Radha et al., 2017). Increased surface pores in composite structures indicate improved mechanical properties and strong adsorption (Kang et al., 2016; Kim et al., 2004).

The Surface Activity Analysis

Figures 5, 6 and 7 show the surface activities of the synthesized composites against *E. coli, L. monocytogenes, Salmonella* and *S. aureus*, respectively. Table 4 gives the results of surface activity analysis.

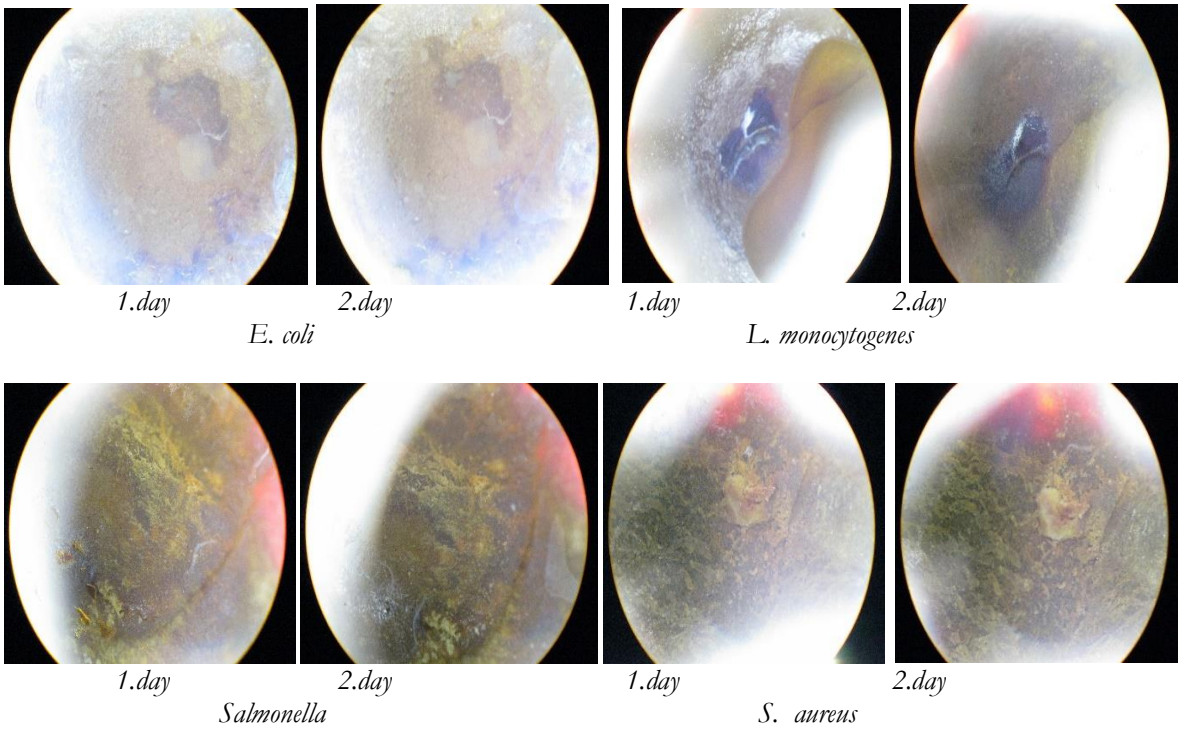

Figure 5. The surface Activity against bacteria *E. coli*, *L. monocytogenes*, *Salmonella* and *S. aureus* of nanocomposite 1

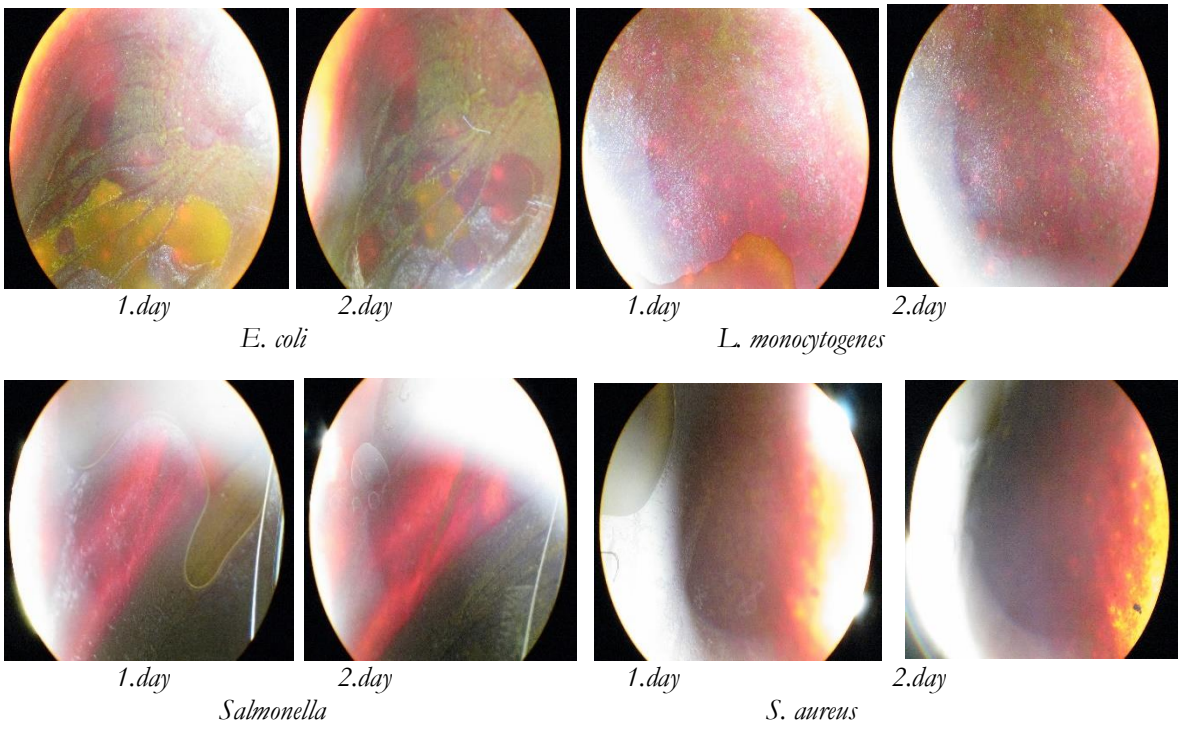

Figure 6. The surface Activity against bacteria *E. coli, L. monocytogenes, Salmonella* and *S. aureus* of nanocomposite 2.

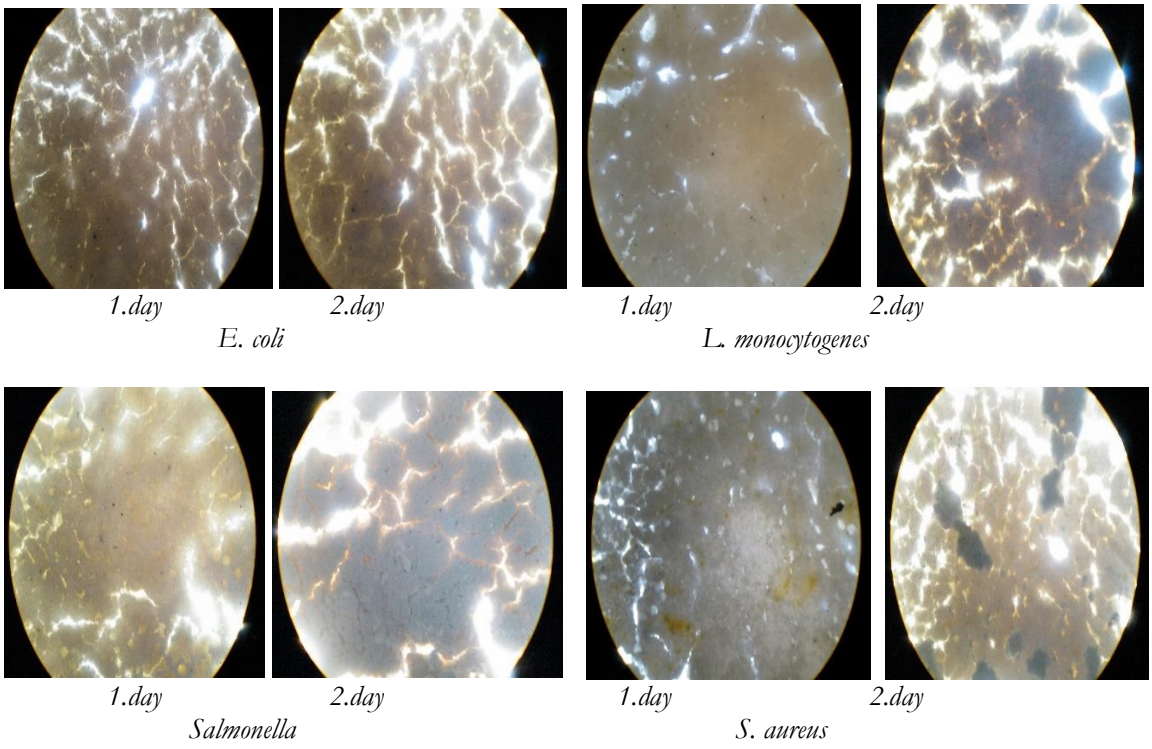

Figure 7. The surface Activity against bacteria *E. coli, L. monocytogenes, Salmonella* and *S. aureus* of nanocomposite 3.

Table 4. The surface activity analysis of the nanocomposites

	E. coli	*L. monocytogenes*	*Salmonella*	*S. aureus*
Composite 1	+	+	-	-
Composite 2	-	-	+	-
Composite 3	+	+	+	+

*Note: + denotes the presence

According to the results of surface activity analysis, nanocomposite 3 structure shows the highest activity against *E. coli, L. monocytogenes, Salmonella*, and *S. aureus*. Nanocomposite 1 and 2 contain a curcumin extract in the chemical composition, while nanocomposite 3 contains the allicin extract. This result confirms that the allicin extract has a stronger surface activity than the curcumin extract. According to this result, nanocomposite 1 and nanocomposite 2 showed stronger mechanical properties and flexibility, because no cracking or cracking occurred on the <Figure 8 and Table 5> surfaces. In the surface of nanocomposite 3 was observed to have very deep cracks and fractures. According to this result, it can be said that the monomer 1 compound increases the mechanical stability of the nanocomposites.

Antibacterial Analysis

Figure 8 and Table 5 show the antibacterial resistance of monomer 1 and Ag^{+}-Mt-Cr against bacteria *E. coli, S. aureus,, L. monocytogenes* and *Salmonella*.

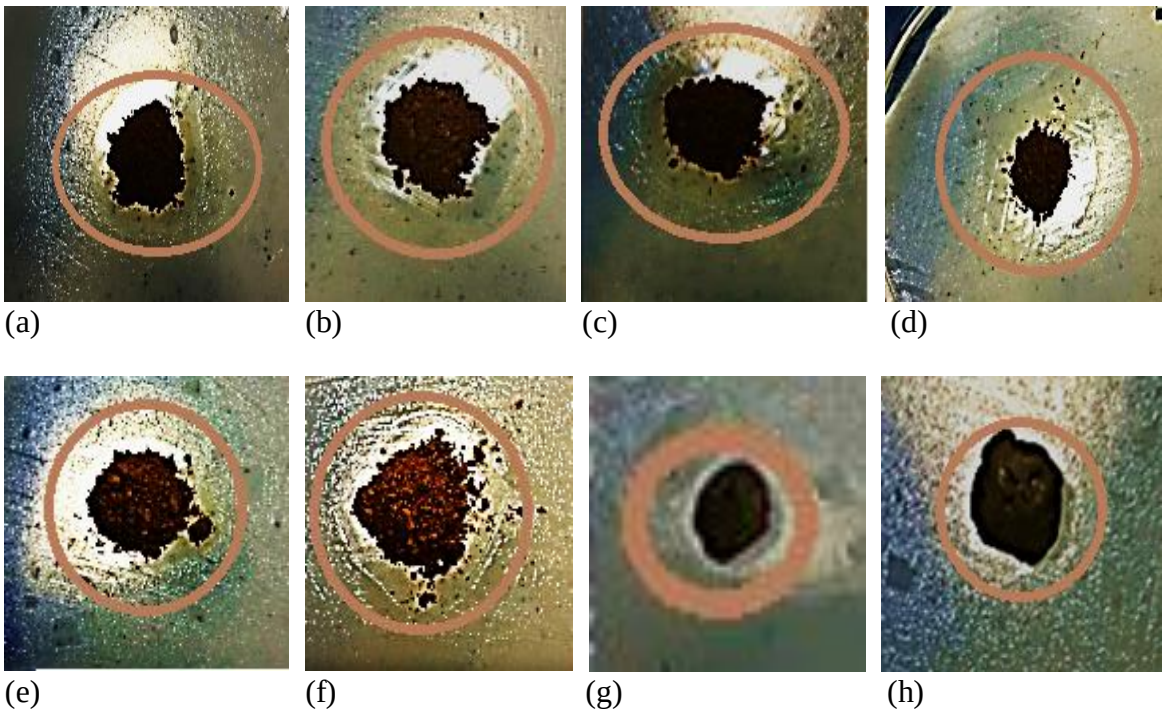

Figure 8. The inhibition zones against bacteria *E. coli (a), S. aureus* (b), *Salmonella (c) ve L. monocytogenes* (d) of Ag^{+}-Mt-Cr, *E. coli (e) and Salmonella* (f), *S. aureus (g), L. monocytogenes (h)* of monomer 1.

Table 5. The inhibition zones of the samples (mm)

	E. coli	*S. aureus*	*Salmonella*	*L. monocytogenes*
Ag^{+}-Mt-Cr	$10^{\alpha} \pm 0.26$	$12^{\alpha} \pm 0.23$	$16^{\alpha} \pm 0.38$	$14^{\alpha} \pm 0.27$
Monomer 1	$4^{\alpha} \pm 0.12$	$2.8^{\alpha} \pm 0.05$	$6^{\alpha} \pm 0.15$	$3.5^{\alpha} \pm 0.08$

* The test was done in triplicate. Data are mean of triplicate measurements±SD. Alphabetical letter in the columns indicate significant ($P \leq 0.05$) differences between means in Tukey's test.

According to the results of antibacterial analysis, Ag^{+}-Mt-Cr showed very high resistance to bacteria. In particular, It showed an 16±0.38 and 14±0.27 mm inhibition zones against *Salmonella* and *L. monocytogenes* bacteria according to Table 5. However, antibacterial resistance decreased with the addition of POSS to the chemical composition. According to experiments, the curcumin showed stronger antibacterial effect when used alone. POSS has a hydrophobic surface and was added to the formulation of composites. This causes the intermolecular interaction of the polymeric network due to the plasticizing effect of absorbed water molecules penetrated between the chain segments. However, it can also lead to reduced contact surface by preventing curcumin extract from reaching the bacterial cell membrane (Bordianu et al., 2012). This result may have caused to decrease of antibacterial properties. Besides, analysis of variance table (One way ANOVA) and Tukey test for differences between means demonstrated statistical significance of the data ($P \leq 0.05$).

Biocompatibility Analysis

After 24 and 72 h of treatment, data showed that the percentage of cell viability increased from 8 to 15% for composite 1 and from 15 to 18% for composite 2, respectively. The cell viability results correlated with PEG amount confirmed that composite 2 showed better biocompatibility. As the amount of PEG increased twice, the

biocompatibility increased at the same rate (Marinescu et al., 2019). Figure 9 shows the effect of treatment with nanocomposites on cell viability of L929 fibroblast cells assessed by MTT.

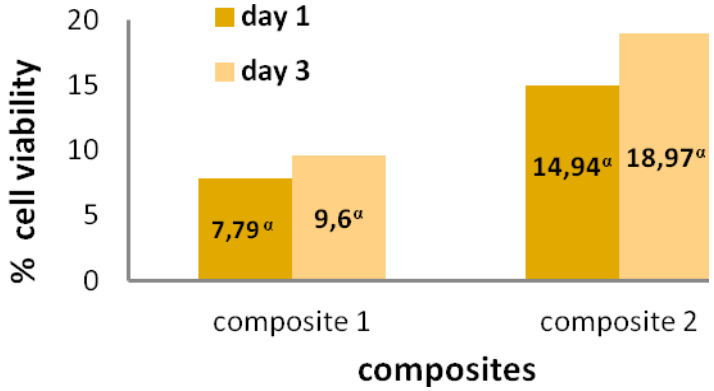

Figure 9. The effect of treatment with nanocomposites on cell viability of L929 fibroblast cells assessed by MTT.

Compared with the literature, the biocompatibility values of PMMA increased to 20% with Sr5-HA (strontium-substituted hydroxyapatite) for 7 days (Lam et al., 2011), In this study, a biocompatibility rate of 9.6 ±0.39 % and 18.97 ±0.77 % for 3 days was obtained for composites 1 and 2, respectively. Analysis of variance table (One way ANOVA) and Tukey test for differences between means demonstrated statistical significance of the data ($P \leq 0.05$).

CONCLUSIONS

In this study, new surface-active nanocomposites were synthesized. After synthesis of monomer 1, new material was synthesized with MMA, curcumin, allicin and Ag^+-montmorillonite and monomer 1. The synthesized new nanocomposites were analyzed for their surface activity against *E. coli, L. monocytogenes, Salmonella* and *S. aureus* bacteria and biocompatibility tests were carried out. Antibacterial resistance of the synthesized monomer 1 and Ag^+-Mt-Cr against *E. coli, L. monocytogenes, Salmonella* and *S. aureus* bacteria were analyzed by the well diffusion method. The analysis results confirmed that the nanocomposites obtained showed surface activity against both gram-negative and gram-positive bacteria. The new compounds synthesized showed the highest inhibition zones against salmonella and L. monocytogenes bacteria at 16±0.38 and 14±0.27 mm, respectively. According to results, the increase in the amount of PEG in the nanocomposite structure increased biocompatibility at the same rate. Increasing the amount of PEG will increase the percent cell viability to higher rates for nanocomposites. Besides, in the article studies, it was seen that the allicin did not cause unwanted odors in the composite synthesis and the migration values were quite below the reference values (Baysal and Doğan, 2020). The reason it did not cause unwanted odors was the addition of limited amounts of reactions. As the amount of allicin used increases, it has the risk of causing unwanted odors.

ACKNOWLEDGMENT

This study was carried out with the support of the Istanbul Aydin University Scientific Research Project. Project number: 27/06/2018-10.

REFERENCES

Abdel Rehim, M.H., Yasin, M.A., Zahran, H., Kamel, S., Moharam, M.E., Turky, G. (2020). Rational design of active packaging films based on polyaniline-coated polymethyl methacrylate/nanocellulose composites. *Polym Bull*, 77(5): 2485- 2499.

Baysal, G., and Çelik, B.Y. (2018). Synthesis and characterization of antibacterial bio-nano films for food packaging. *J Envıron Sci Heal B*, DOİ: 10.1080/03601234.2018.1530546.

Baysal, G., and Doğan, F. (2020). İnvestigation and preparation of biodegradable starch-based nanofilms for potential use of curcumin and garlic in food packaging applications. *J Biomater Sci Polym Ed,* 31(9): 1-17

Bordianu, I.E., David, G., Simionescu, B., Aflori, M., Ursu, C., Coroaba, A., Hitruc, G., Cotofana, C., Olaru, M. (2012). Functional silsesquioxane-based hierarchical assemblies for antibacterial/antifungal coatings. *J Mater Chem B,* 00: 1-5.

Cheng, H., and Huang, G. (2018). Extraction, characterisation and antioxidant activity of allium sativum polysaccharide. *Int J Biol Macromol,* 114: 415–419.

Dag, D., Guner, S., Halil Oztop M. (2019). Physicochemical mechanisms of different biopolymers (lysozyme, gum arabic, whey protein, chitosan) adsorption on green tea extract loaded liposomes. *Int J Biol Macromol*, 138: 473–482.

Deng, F., Li, M.C., Ge, X., Zhang, Y., Cho, U.R. (2017). Cellulose nanocrystals/poly(methyl methacrylate) nanocomposite films: Effect of preparation method and loading on the optical, thermal, mechanical, and gas barrier properties. *Polym Compos*, 38: E137- E146.

Dhivya, R., Ranjani, J., Bowen, P. K., Rajendhran, J., Mayandi, J., Annaraj, J. (2017). Biocompatible curcumin loaded PMMA-PEG/ZnO nanocomposite induce apoptosis and cytotoxicity in human gastric cancer cells. *Mater Sci Eng C*, 80: 59–68.

Kang, T., Hua, X., Liang, P., Rao, M., Wang, Q., Quan, C., Zhang, C., Jiang, Q. (2016). Synergistic reinforcement of polydopamine-coated hydroxyapatite and BMP2 biomimetic peptide on the bioactivity of PMMA-based cement. *Compos Sci Technol,* 123:232-240.

Kim, S.B., Jick Kim, Y., Lim Yoon, T., Park, S.U., Cho, I.H., Kim, E.J., Kima, I.A., Shin, J.W. (2004). The characteristics of a hydroxyapatite–chitosan–PMMA bone cement. *Biomaterials*, 25: 5715–5723.

Lam, W.M., Pan, H.B., Fong, M.K., Cheung, W.S., Wong, K.L., Li, Z.Y., K. Luk, K.D., Chan, W.K., Wong, C. Yang, C.T., Lu, W.W. (2011). In Vitro characterization of low modulus linoleic acid coated strontiumsubstituted hydroxyapatite containing PMMA bone cement. *J Bıomed Mater Res B,* 96B(1): 76-83

Marinescu, C., Sofronia, A., Anghel, E.M., Baies, R., Constantin, D., Seciu, A.M., Gingu, O., Tanasescu, S. (2019). Microstructure, stability and biocompatibility of hydroxyapatite -titania nanocomposites formed by two step sintering process. *Arab J Chem*, 12: 857–867.

Özçelik, S., Sümer, Z., Değerli, S., Ozan, F., Sökmen, A. (2007). Garlic (Allium Sativum) extract scolocidal can be used as agent. *Turkiye Parasitol Derg*, 31 (4): 318-321.

Philip, P., Tomlal Jose E., Chacko, J K., Philip, K.C., Thomas, P.C. (2019). Preparation and characterisation of surface roughened PMMA electrospun nanofibers from PEO-PMMA polymer blend nanofibers. *Polym Test*, 74: 257–265.

Radha, G., Balakumar, S., Venkatesan, B., Vellaichamy, E. (2017). A novel nano-hydroxyapatite-PMMA hybrid scaffolds adopted by conjugated thermal induced phase separation (TIPS) and wet-chemical approach: Analysis of its mechanical and biological properties. *Mater Sci Eng C*, 75: 221–228.

Ravindar Reddy, M., Subrahmanyam, A. R., Maheshwar Reddy, M., Siva Kumarc, J., Kamalaker, V., and Jaipal Reddy, M. (2019). X-RD, SEM, FT-IR, DSC Studies of polymer blend films of PMMA and PEO. *Mater Today: Proceedings,* 3: 3713–3718.

Rostami, M.R., Yousefi, M., Khezerlou, A., Aman Mohammadi, M., Jafari, S.M. (2019). Application of different biopolymers for nanoencapsulation of antioxidants via electrohydrodynamic processes. *Food Hydrocoll,* 97: 105170.

Shinzawa,H., and Mizukado, J. (2018). Rheo-optical near-infrared (NIR) spectroscopy study of

partially miscible polymer blend of polymethyl methacrylate (PMMA) and polyethylene glycol (PEG). *Spectrochim Acta A Mol Biomol Spectrosc*, 192: 236–243.

Silva, M.N., Fonsecaa, J.M., Feldhaus, H.K., Soares, L.S., Valencia, G.A., Maduro de Campos, C.E., Di Luccio, M., Monteiro. A.R. (2019). Physical and morphological properties of hydroxypropyl methylcellulose films with curcumin polymorphs. *Food Hydrocoll*, 7: 105217.

Sohrabnezhad, S., Rassa, M., Mohammadi Dahanesari, E. (2016). Spectroscopic study of silver halides in montmorillonite and their antibacterial activity. *J Photoch Photobio B,* 163:150-155. Doi: 10. 1016/j.jphotobiol.2016.08.018.

Söğüt, E., Seydim, A.C. (2017). Bio-based nanocomposıtes and applıcatıons ın food packaging. *The Journal of Food,* 47(6): 821-833.

Yalcin, B., Cakmak, M., Arkın, A.H., Hazer, B., Erman, B. (2006). Control of optical anisotropy at large deformations in PMMA/chlorinated PHB (PHB-Cl) blends: Mechano-optical behavior. *Polymer*, 47: 8183-8193.

Zhao, F., Wan, C., Bao, X., Kandasubramanian, B. (2009). Modification of montmorillonite with aminopropylisooctyl polyhedral oligomeric silsequioxane. *J Colloid Interface Sci,* 333:164–170.